Electrocatalysis under Conditions of High Mass Transport: Investigation of Hydrogen Oxidation on Single Submicron Pt Particles Supported on Carbon

Shengli Chen and Anthony Kucernak*

Department of Chemistry, Imperial College London, London SW7 2AZ, United Kingdom

Received: March 27, 2004; In Final Form: June 15, 2004

The mechanism and kinetics of the hydrogen oxidation reaction (*hor*) has been investigated using carbon-supported single particles of Pt electrocatalyst with radii as small as 40 nm. The high mass transport rates on such small particles enable us to investigate the rapid kinetics of the *hor* in the absence of diffusion limitations. Surface kinetic controlled polarization curves during the electrochemical oxidation of hydrogen molecules in acid solution have been obtained in the entire H UPD region, showing features obviously different from those obtained on normal micrometer electrodes or in RDE experiments. For instance, two current plateaus rather than one are seen during the steady-state polarization of the *hor* on electrodes made of small particles. Upon decreasing the size of the Pt particles, the two current plateaus show greater separation and become better defined. A theoretical model for the steady-state polarization of the *hor* has been developed in which UPD H atoms of various states are considered as the reactive intermediates and the Frumkin adsorption mode is assumed for the atomic H on Pt electrodes. It is shown that the first current plateau represents the limiting reaction rate under adsorption or combined adsorption−diffusion control while the second plateau current corresponds to the limiting diffusion-controlled reaction rate. It is pointed out that Tafel plots that have been frequently used for kinetics analysis in the *hor* are meaningless, especially in the potential region below 0.05V vs RHE. The polarization curves are fitted with a general polarization equation derived according to our model. The fitting shows that the *hor* on Pt proceeds most likely via the Tafel−Volmer reaction mechanism rather than the Heyrovsky−Volmer mechanism. These results have significant implications on the understanding and modeling of the reactions in solid polymer electrolyte fuel cells.

1. Introduction

The hydrogen oxidation reaction (*hor*) is one of the most important reactions in both fundamental and applied electrochemical science, particularly in connection with fuel cells. Compared to the oxygen reduction reaction (*orr*) occurring on the cathode of fuel cells, the *hor* that takes place on the anodic side of fuel cells is rarely investigated, especially as far as reaction kinetics is concerned. This is because the anode contributes very little to the activation polarization under typical fuel cell operating conditions since the *hor* has a much larger value of the exchange current density j_0 than the *orr*.[1] In most of the experimental and theoretical studies on fuel cells, the polarization of the anode has been considered negligible unless the operating current density is high enough so that mass transport polarization effects arise on the anode. Furthermore, the fast reaction rate of the *hor* also renders the study of its kinetics rather difficult due to the relatively slow mass transport of H_2 in most of the electrochemical methods used to study this reaction. Rotating electrode techniques (e.g., RDE) are usually used to increase the mass transport rate in electrochemical studies.[2] Indeed, RDE methods have been employed in a number of studies attempting to extract kinetic information about the *hor*.[3−9] It has been frequently argued, however, that the rate of the *hor* on the Pt electrode in acid solution might be too fast to be measured with the RDE method.[3,6,10] To get reliable information on the dependence of the *hor*/*her (hydrogen evolution reaction)* kinetics on the crystallographic orientation of the platinum surface atoms, Marković et al.[5−7] had to conduct the measurements at lower temperatures or in alkaline media where the j_0 value is significantly decreased. The RDE measurement at low temperatures performed by these authors did reveal information about the effects of surface crystallography on the *hor* kinetics on Pt electrodes in acid solution that were missed in normal RDE studies by others.[6,11,12] So far, there remain a number of open questions with regard to the kinetics and mechanism of the electrochemical oxidation of hydrogen molecules in the electrolyte solution.

Although it is well accepted that the electrooxidation of hydrogen at Pt in acid solution is a very fast reaction, the question may be posed "how fast?". The values of j_0 (or the standard kinetics rate constant, k_0) for the *her*/*hor* on Pt in acid solution show a large scatter in the literature. Table 1 gives some reported values of j_0 or k_0, which can be calculated from each other according to eq 1,[13]

$$j_0 = 2Fk_0c_{H_2^*} \tag{1}$$

where $c_{H_2^*}$ ($\sim 5.9 \times 10^{-7}$ mol cm^{-3}) is the concentration of hydrogen in bulk solution.[9] The measurement conducted with the RDE method at room temperatures mostly gave j_0 values of about 1 mA cm^{-2}, while j_0 values of several tens of mA cm^{-2} were frequently obtained in measurements with other techniques. The accessible mass transport rate in RDE methods is limited by the onset of turbulent flow and vortex formation at rotation rates above 10 000 rpm.[2] The measurements done

* Address correspondence to this autho. Phone: +44 20 75945831. Fax: +44 20 75945804. E-mail: a.kucernak@imperial.ac.uk.

10.1021/jp048641u CCC: $27.50
Published on Web 08/21/2004

TABLE 1: Selection of Literature-Reported Values of Exchange Current Density j_0 and Standard Kinetics Rate Constant k_0

method	medium (temp/°C)	j_0/mA cm^{-2}	k_0/cm s^{-1}
RDE[6]	0.05 mol dm^{-3} H_2SO_4 (30 °C)	0.98[a]	~0.006
RDE[11]	0.5 mol dm^{-3} H_2SO_4 (rt[b])	~1.4[a]	~0.01
RDE[8]	0.1 mol dm^{-3} $HClO_4$ (rt[b])	1.35	~0.01
microelectrode + thin liquid layer[10]	0.5−1 mol dm^{-3} H_2SO_4 (25 °C)	>50	>0.25
rapid potentiodynamic scanning[13]	96% H_3PO_4 (22 °C)	27	0.14
SECM[14]	0.01 mol dm^{-3} $HClO_4$ + 0.1 mol dm^{-3} $NaClO_4$ (rt[b])	~42	0.22
SECM[15]	0.01 mol dm^{-3} $HClO_4$ + 0.1 mol dm^{-3} $NaClO_4$ (rt[b])	60−80	0.3−0.4

[a] Obtained on Pt(110) that was shown to be the most active crystal plane for the *hor* in acid solution.[6] [b] rt = room temperature.

in refs 6 and 11 were conducted at rotation rates of about 1000 rpm. The mass transport coefficient for the RDE method is[2]

$$m = 0.62D^{2/3}\upsilon^{-1/6}\omega^{1/2} \tag{2}$$

where D is the diffusion coefficient, which is about 3.7×10^{-5} cm^2 s^{-1} for hydrogen in sulfuric acid solution.[6] υ ($\approx 1.1 \times 10^{-2}$ cm^2 s^{-1}) is the kinetic viscosity of that electrolyte. ω is the rotation rate. The value of m for the hydrogen molecule is about 0.015 cm s^{-1} at a rotation rate of 1000 rpm. Assuming that the exchange current density of the *hor* is 20 mA cm^{-2}, which corresponds to a standard rate constant k_0 of 0.18 cm s^{-1} according to eq 1, then we have

$$\lambda = \frac{k_0}{m} > 10 \tag{3}$$

The parameter λ, the ratio between the standard rate constant of a electrode reaction and the mass transport coefficient of the measuring system, is a criterion of the relative reversibility of an electrode process.[16,17] In general, a λ value of 10 or greater suggests that the electrode process is totally reversible and it is impossible to extract kinetic information from steady-state measurements.[17] Indeed, pure diffusion-controlled polarization behavior has been mostly obtained for the *hor* on Pt electrodes in acid solution in RDE measurements.[3,4,9,10,18] Harrison et al.[3] found that the *hor* in 0.5 mol dm^{-3} H_2SO_4 on Pt electrodes exhibits completely diffusion-controlled polarization behavior even when using an RDE at a rotation rate up to about 7000 rpm. They concluded that the exchange current density of the hydrogen reaction must be greater than 0.5 A cm^{-2}. To more accurately investigate the reaction kinetics of hydrogen oxidation, transient techniques such as rapid potentiodynamic scanning[13] or other steady-state methods that allow high mass transport need to be used. Bagotzky et al.[10] employed a combined microelectrode and thin-liquid-layer method to study the *hor* on Pt electrodes, in which a Pt microelectrode about 100 μm in diameter was placed in the thin meniscus zone above an electrolyte. By comparing their polarization data with the ideal diffusion-controlled polarization curve, they concluded that the exchange current density for the *hor* at Pt in acid solution must not be less than 5×10^{-2} A cm^{-2}.[10] Recently,the Scanning Electrochemical Microscopy (SECM) method has been used in the studies of the *hor*.[14,15,19] The SECM method promises steady-state measurements of fast heterogeneous kinetics by placing the tip of an ultramicroelectrode very close to a substrate, utilizing both the microelectrode and the thin electrolyte liquid layer to attain a high mass transport rate.[20]

The *hor* predominantly proceeds in potentials more positive than the potential of the reversible hydrogen electrode (RHE) where the so-called underpotential deposition (UPD) of hydrogen on Pt occurs. This process is manifested by the current peaks in the cyclic voltammograms of Pt electrodes in acid solution free of hydrogen molecules.

An interesting question concerns the role that the H_{upd} may play in the electrochemical oxidation of hydrogen molecules. It is believed that the electrocatalytic oxidation of hydrogen molecules on Pt essentially also involves atomic H in a chemisorbed state (Pt-H_{chem}) as a reactive intermediate.[13,21,22] There is significant discussion in the literature as to the nature of Pt-H_{chem}, and currently there are two viewpoints in the literature. In one, H_{upd} is the intermediate involved in the oxidation of dihydrogen as suggested by Conway et al.,[22] in the other some other form of adsorbed hydrogen acts as the intermediate and H_{upd} acts as a blocking intermediate.[5−7]

At this point it is useful to compare the situation during the hydrogen evolution reaction (*her*). During the *her* at potentials negative of the reversible potential, overpotential deposited hydrogen, $H_{opd,}$ is considered to be the active intermediate.[22−27] It is generally accepted that the H_{opd} produced during the *her* is a distinctly different species from H_{upd} based on experimental spectroscopic evidence showing that H_{opd} interacts with water molecules forming a bond whereas H_{upd} does not.[28−31] The fact that H_{opd} and H_{upd} coexist at negative potentials and must occupy distinct surface adsorption sites is also supported by other evidence.[32,33]

By analogy with the *her* some believe that H_{opd} or some form of hydrogen quite similar to it is the intermediate during the *hor*. For instance, Marković et al. believe that H_{opd} serves as an intermediate in both the *her* and *hor*, at least near the equilibrium potential.[5−7] The OPD H in their definition thus should be some kind of weakly adsorbed hydrogen atom, not necessarily formed only at potentials negative of the equilibrium potential. They suggested that UPD H may act as an inhibitor to the *hor* by blocking surface sites. As discussed above, RDE measurements of the *hor* at room temperature exhibit almost reversible polarization behavior with limiting diffusion behavior occurring once the potential is positive of 0.05 V (RHE). This makes it impossible to study the reaction kinetics and mechanism of the *hor* in the UPD H region. To reveal the role of UPD H in the *hor* high mass transport rates are required to delay the occurrence of complete concentration polarization. If this is achieved then the *hor* is under kinetic or partially kinetic control in the UPD H region.

The most efficient and straightforward way to increase the mass transport rate would be by decreasing the size of the electrode used so that it attains micron and even submicron dimensions. The mass transport coefficient for a microelectrode with radius r is given as[16,17]

$$m = \frac{HD}{r} \tag{4}$$

where the coefficient H depends on the shape of the exposed portion of the microelectrode, and is 1 for a hemispherical microelectrode and $4/\pi$ for a disk-shaped microelectrode. The mass transport coefficient of the rotating disk experiments mentioned above (ω = 1000 rpm) is 0.015 cm s^{-1}; this could

be achieved at an electrode of 25 μm in radius. Clearly, for smaller electrodes, we will quickly exceed the maximum mass transport rates achievable with a rotating disk electrode. For example, a hemispherical microelectrode with radius of 1 μm allows mass transport rates of greater than 0.37 cm s^{-1}. To obtain an equivalent mass transport rate at a rotating disk electrode a rotation rate of almost 10^6 rpm would be required. Clearly this is impractical, as rotating disk measurements are limited by cavitation in the electrolyte, which typically occurs around 10 000 rpm. Although small Pt electrodes of even nanometer size can be fabricated by etching Pt microwires followed by insulation of the major proportion of the platinum surface,[34−36] the application of such small electrodes in heterogeneous electrocatalysis is difficult because the surface of the electrodes produced in this manner may be contaminated by the materials used for insulation. An uncontaminated electrode surface is crucial in heterogeneous electrocatalysis studies.

Recently, we have developed a method to prepare electrodes made of individual Pt particles supported on small carbon substrates. The principle used to produce such small Pt particle electrodes is that when a substrate has an electroactive area comparable in size to that of a stable nuclei of metal clusters (typically about 1 nm) or the depletion layer around it, the electrodeposition may proceed via a single nucleation and growth mechanism, leading to formation of a single supported metal particle. We have demonstrated that very small carbon electrodes can be fabricated by insulating etched carbon fibers with electrophoretic paint.[37,38] The potentiostatic deposition of Pt on these small carbon electrodes clearly showed current transients associated with single nucleation and growth processes. The resulting Pt particles sit on the top end of the insulated carbon tip and have approximately hemispherical shape.[39] By terminating the deposition after a specified charge has been consumed, particles of Pt with radius ranging from a few tens of nanometers to several micrometers can be reproducibly produced. Such carbon-supported Pt particle electrodes may act as model catalyst particles in the study of fuel cell relevant reactions without the complication of the presence of other nearby catalyst particles allowing measurements under conditions of defined mass transport and kinetics. The small surface area of the supporting electrode means that the response of the Pt particle is not swamped by background electrochemistry occurring on the substrate. As these Pt particles are deposited after the insulation process, the Pt surface remains unadulterated and uncontaminated. The high mass transport rates at very small single particles enable us to investigate the kinetics of rapid heterogeneous electrocatalytic processes under steady-state conditions without the results being compromised by diffusional effects. Previously, we have used these small Pt particle electrodes to study the oxygen reduction reaction on platinum under conditions of high rates of mass transport and to model the resulting response.[40] In this paper, we use these single Pt particle electrodes to study the *hor* in acid solution. On electrodes composed of a single Pt particle of submicrometer dimension, steady-state polarization curves associated with kinetic-controlled electrode processes are obtained in the entire H UPD region, allowing the investigation of the role of UPD H atoms in the *hor*. The approach developed also explains the wide scatter of values for the exchange current density of the hydrogen oxidation reaction.

2. Experimental Section

H_2SO_4 (Merck, Aristar), H_2PtCl_6 (Aldrich, 99.9%), $Ru(NH_3)_6Cl_3$ (Aldrich, 98%), and KCl (BDH Analar) were used. All solutions were prepared with Milli-Q water. All the experiments are conducted at a temperature of 23 ± 1 °C.

2.1. Electrode Preparation. 2.1.1. Carbon-Supported Single Pt Particle Electrodes. The carbon substrate electrodes are prepared through electrochemical etching of carbon fibers (PANEX33 CF, 95% Carbon, unsized, Zoltek Corporation, MO) followed by deposition of cathodic electrophoretic paint (Clearclad HSR, LVH coating Ltd, UK) to insulate the etched fibers. A new deposition procedure, the so-called inverted deposition approach is employed, which allows the insulation of the bulk of the etched fiber while keeping the tip end free of insulation.[37,38] The exposed electroactive area of these carbon electrodes can be very small, e.g., down to a few nanometers in radii, as indicated by the steady-state limiting current during the reduction of 0.01 mol dm^{-3} of $Ru(NH_3)_6Cl_3$ in 0.5 mol dm^{-3} of KCl. The Pt electrodeposition solution was 0.1 mol dm^{-3} of $H_2SO_4 + 1 \times 10^{-3}$ mol dm^{-3} of H_2PtCl_6. Pure argon gas was bubbled into the electrodeposition solution for 15 min to remove any oxygen prior to each deposition experiment. During the deposition, an argon atmosphere was maintained above the solution. The Pt was deposited at −0.1 V vs SCE at which potential the deposition process occurs under limiting diffusion control.[39] Before and after deposition of Pt, the electrodes were thoroughly rinsed with a large amount of Milli-Q water. SEM images of the resultant Pt−carbon composite electrodes show that the Pt particles sit at the top end of the insulated carbon tips and have approximate hemisphere shapes.[39] These particles are almost uniformly accessible for diffusion and the corresponding diffusion geometries around such particles are between a hemisphere and a sphere. So, the mass transport coefficient of these particles can be defined by using eq 4.

2.1.2. Pt Microdisk Electrodes. Pt microdisk electrodes, used to calibrate the hydrogen concentration and diffusion coefficient in solutions, were made by sealing Pt microwires (Goodfellow) into tapered glass tube, using a resistive heating coil made from Nichrome wire (Advent, Ni80/Cr20, 0.5 mm in diameter). The Pt disk was exposed by polishing on 30 μm alumina paper. After the Pt was exposed, the electrodes were then polished with 9-, 1-, and 0.3-μm alumina paper, respectively. Each time before an electrode was used they were polished with 0.3-μm alumina paper and ultrasonically rinsed in Milli-Q water. Following this the electrodes were immersed in acidified potassium permanganate solution for 30 min followed by an ultrasonic clean in acidified dilute H_2O_2 solution, Milli-Q water, and 0.1 mol dm^{-3} of H_2SO_4, respectively.

2.2. Electrochemical Measurement. An AutoLab PGSTAT20 potentiostat with the ECD module (Eco Chemie BV, Netherlands) was used in all electrochemical experiments. A two-electrode configuration was employed in the experiments using Pt particle electrodes. As counter electrode a calomel reference electrode was employed in the experiments for determining the electroactive radii of carbon electrodes and for electrodeposition of platinum. A large Pt sheet was used as a combined counter and quasireference electrode in the experiments for hydrogen oxidation. In the experiments using Pt microdisk electrodes, a three-electrode configuration was used with a RHE as reference electrode and a large Pt sheet as counter electrode. The potentials are reported with respect to RHE in this paper. The glass electrochemical cell and the Pt quasireference electrode were immersed in acidified potassium permanganate solution overnight and rinsed with acidified dilute H_2O_2 solution and Milli-Q water respectively before use.

After being rinsed with a large amount of water and then with a 0.1 mol dm^{-3} H_2SO_4 solution, the Pt particle electrodes

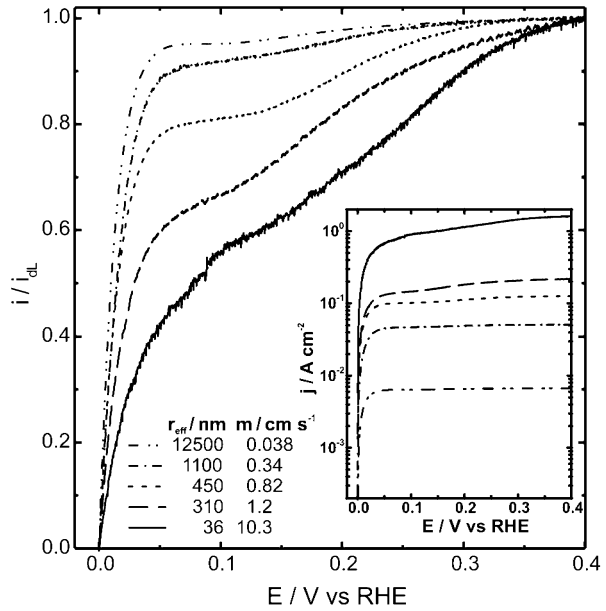

Figure 1. The current−potential curves obtained on Pt particle electrodes accompanying the oxidation of hydrogen in 0.1 mol dm^{-3} H_2SO_4 solution saturated with CO free hydrogen gas. The current are normalized by the limiting values read at about 0.45 V. The numbers in the figure indicate the particle radius, and give the mass transport rate for that particle assuming a hydrogen diffusion coefficient of 3.7 $\times$ 10^{-5} cm s^{-1}. Scan rate = 5 mV s^{-1}.

were transferred into the electrochemical cell containing 0.1 mol dm^{-3} of H_2SO_4 saturated with high purity argon and subjected to potential cycling between 0.05 and 1.45 V with a scan rate of 100 mV s^{-1} until reproducible and well-defined CVs were obtained. The solution was then replaced by fresh 0.1 mol dm^{-3} H_2SO_4 and CO free hydrogen gas (research grade) was bubbled through the solution for at least 20 min. The electrodes were then again subjected to several cycles of potential scan (0.05−1.45 V) until the CVs became reproducible. Immediately after this cycling, a steady-state current−potential curve (1.4−0.02 V) was recorded at a scan rate of 5 mV s^{-1}. The steady-state polarization curves were recorded starting from a positive potential so that a freshly reduced and clean electrode surface is maintained. During the experiments, an atmosphere of hydrogen was kept in the cell above the solution. The size of the Pt particle is estimated from the limiting diffusion current for H_2 oxidation according to eq 5 by assuming that the particle has a hemispherical shape

$$j_{dL} = 2Fmc_{H_2^*} \quad (5)$$

where j_{dL} represents the limiting diffusion current density. m and $c_{H_2^*}$ are defined above.

3. Results and Discussion

3.1. The Steady-State Polarization Curves of hor on Pt Particle Electrodes. Figure 1 shows the steady-state current−potential profiles for hydrogen oxidation obtained on carbon-supported Pt particles of different size. The current is normalized to the corresponding limiting value seen at potentials more positive than 0.4 V. The inset in this diagram is the current density−potential plot for each of these particles. The surface area of the particles used to calculate the current density is the surface area calculated from the charge involved in the hydrogen adsorption/desorption current peaks on the cyclic voltamograms obtained in the solution of 0.1 mol dm^{-3} of H_2SO_4. These surface areas are close to those expected if the particles have a morphology between a hemisphere and a sphere. The limiting current densities vary by almost 3 orders of magnitude for the range of particle sizes examined. It can be seen that the steady-state voltammetric curves obtained on electrodes made of smaller Pt particles show obviously different features from those obtained in RDE experiments. On the polarization curves for *hor* obtained in RDE measurements at room temperatures, the steady-state current generally rises sharply from the origin with positive going potential and reaches a limiting plateau above 0.05 V. The fact that these experiments are performed in a significantly different regime from the common rotating disk experiments is illustrated in Table 2, where the calculated mass transport coefficients for the electrodes (using eq 4) are plotted, as well as the disk rotation rates necessary to produce the same mass transport coefficients in a rotating disk experiment (eq 2).

TABLE 2: Variation of Mass Transport Coefficient for Hydrogen as a Function of Electrode Size Calculated by Using Eq 4, Assuming a Hemispherical Shape and D_{H_2} = 3.7 $\times$ 10^{-5} cm^2 s^{-1} [a]

electrode radius/nm	m/cm s^{-1}	ω/rpm
36	10.3	4.6×10^8
310	1.2	6.1×10^6
450	0.82	2.9×10^6
1100	0.34	4.8×10^5
12500	0.038	6100

[a] The equivalent rotation rate, ω, required to produce the same mass transport coefficient for hydrogen in a rotating disk experiment is also displayed.

On the small particle electrodes, two limiting current plateaus with different plateau values can be seen on the steady-state polarization curves for *hor*, seemingly indicating that there are two separate processes involved in the electrochemical oxidation of H_2 in the solution that reach the limiting rate at different potentials. The lower potential current plateau is established at potentials more positive than 0.05 V and extends for about 100 mV. The potential where the second current plateau appears depends on the size of the particle. The smaller the particle radius, the more positive a potential is required for the current to reach the second limiting plateau. The two current plateaus become less separated upon increasing the electrode size. On electrodes 12.5 μm in radius, the separation between the two limiting current plateaus is almost invisible. They completely merge into one another when a Pt microelectrode of 50-μm diameter was used.

The occurrence of an extra limiting current is also evident on the polarization curves of the *hor* in dilute H_2SO_4 solution on Pt(100) electrodes at a temperature of 274 K performed by Marković et al.,[6] although this feature has not hitherto been commented upon. Bagotzky et al.[10] also mentioned the occurrence of an extra limiting current in their study of *hor* using combined microelectrode and thin liquid layer technique, especially when a very thin liquid layer was employed. They thought it might be due to the increased resistance of the liquid layer since such an extra limiting current became invisible when a thick layer of liquid was employed. Combining the observations from these two studies and those of the present results obtained on small particle electrodes, it is clear that the occurrence of an extra limiting current is a result of a decrease in the value of λ, the ratio between the reaction rate constant and the mass transport coefficient as defined above in eq 3. The decrease in λ value delays the occurrence of the limiting concentration polarization so that the reaction comes under interfacial kinetic control in the potential region where limiting

diffusion occurs at high λ values. The transition between the two limiting current plateaus covers the entire region where the adsorption/desorption of UPD H occurs. This suggests that UPD H may be involved in the electrochemical *hor* in solution.

3.2. The Steady-State Polarization Equation of hor on Pt. In most *hor* studies, the kinetic analysis has been based on the general polarization theories for simple redox reactions.[6,9,14,15,41,42] In reality, the oxidation of hydrogen involves preceding chemical and adsorption processes coupled to the electron-transfer steps and there may be multiple adsorbed species involved in the reaction. It is necessary to have the appropriate polarization equations associated with the full reaction pathways for a realistic kinetic analysis of the *hor*. The electrochemical oxidation of the hydrogen molecule on polycrystalline Pt electrodes in acid solution is considered to proceed through either the Tafel−Volmer mechanism or the Heyrovsky−Volmer mechanism depending on whether the preceding dissociative adsorption step is a pure chemical process (Tafel reaction, eq 6) or a combined chemical−electrochemical process (Heyrovsky reaction, eq 7).[13,21,22] Since the discharge rate of the atomic H on Pt is very high,[43] the dissociative adsorption processes are the rate-determined steps regardless of the reaction mechanism.

$$H_2^s + Pt \underset{k_{1-}}{\overset{k_1}{\rightleftharpoons}} 2Pt\text{-}H_{chem} \text{ (Tafel reaction)} \quad (6)$$

$$H_2^s + Pt \underset{k_{2-}}{\overset{k_2}{\rightleftharpoons}} 2Pt\text{-}H_{chem} + H^+ + e^- \text{ (Heyrovsky reaction)} \quad (7)$$

$$Pt\text{-}H_{chem} \underset{k_{3-}}{\overset{k_3}{\rightleftharpoons}} Pt + H^+ + e^- \text{ (Volmer reaction)} \quad (8)$$

In eqs 6 and 7, H_2^s represents the molecular hydrogen in the vicinity of the electrode surface having approached from the bulk solution by diffusion. When the mass transport rate of the system is much faster than the rate of the dissociative adsorption reaction, the difference between the concentration of H_2^s and the hydrogen in bulk solution (H_2^*) will be negligible and diffusion contributes little to the overall reaction rate. In comparison, when the mass transport rate is low, the diffusion of hydrogen molecules will play a significant role on the reaction rate.

Before we can derive an expression for the current−potential relationship, it is necessary to have a clear picture about the adsorption of hydrogen on the electrode surface since the *hor* occurs in the potential region where UPD H covers the electrode surface.

At potentials positive to the RHE, the reaction occurring in an electrolyte solution containing no molecular hydrogen would be the equilibrium process between the discharge of hydrogen ions (adsorption) to form the so-called UPD H and the ionization of those same adsorbed UPD H (desorption), i.e.

$$Pt\text{-}H_{upd} \underset{k_-}{\overset{k}{\rightleftharpoons}} Pt + H^+ + e^- \quad (9)$$

It can be seen that this equilibrium reaction is almost identical with the Volmer reaction except that the adsorbed H is deliberately labeled by the subscript UPD. It is well-known that there are at least two types of UPD hydrogen on Pt electrodes due to the existence of distinct surface sites, as manifested by the multiple adsorption/desorption peaks in the cyclic voltammograms of Pt in acid solution.[44,45] These multiple states of chemisorbed atomic H are generally called strongly bound H and weakly bound H.[44]

As our experimental approach allows us to study the hydrogen oxidation process over the entire potential region over which H_{upd} exists, in our model we assume that H_{chem} is the same as H_{upd}. If there are surface sites on which the H_{chem} from the dissociation of H_2 can adsorb, they also should be accessible to H_{upd} because both reactions occur in the same potential region. So, it is reasonable to believe that eq 9, the reaction associated with the formation/desorption of H_{upd}, is the same as the Volmer reaction. It is difficult to imagine that these processes are different. In other words, the adsorbed atomic H from either H_2 dissociation or the discharge of the hydrogen ions should be indistinguishable on the electrode surface. Otherwise the Volmer reaction would have a different form from that in eq 8. In fact, the dissociation of hydrogen molecules on Pt in the gas phase also forms two types of surface atomic H, analogous to the different UPD H states.[46,47] It thus seems reasonable that the H_2 in solution should follow the same reaction. Recently, Marković et al. have suggested that in solution H_{chem} is different from H_{upd}, and indeed this latter species inhibits the *hor*.[5−7] Their hypothesis has been based on their results of the *hor* in alkaline and acid solution at very low temperature that show an increase in the reaction rate mirrored by a decrease in the coverage of UPD H. As can be seen from the polarization curves obtained on our small particle electrodes (Figure 1), the *hor* current does increase continuously with increasing potential within the H UPD region. This is consistent with the results obtained by Marković et al., thus seeming to support their hypothesis. But it is physically unreasonable that the atomic H formed after H_2 adsorption at potentials significantly positive of the RHE could be different from H_{upd}. As will be shown in the next section, the increase in hydrogen oxidation current with potential within the UPD H region does not necessarily mean that the UPD H inhibits the *hor*. We can obtain reasonable fits to the polarization curves without distinguishing H_{upd} from H_{chem} formed due to H_2 dissociation. The variation in reaction rate is then due to the variation in coverage of free Pt sites on which the initial adsorption of H_2 can occur (i.e. the Tafel or Heyrovski steps). In agreement with Conway et al.,[22] we consider that the reactive intermediates in *hor* are H_{upd}. Such an approach is also supported by the work of Zolfaghari et al., who find similar bond strengths for H_{chem} and H_{upd}, consistent with the equivalence of these two types of adsorbed hydrogen.[48] Furthermore, we believe that the reactivity of the different forms of UPD H is different. This seems reasonable considering that the adsorbed H have different adsorption strengths and physically occupy different sites. The current density j due to hydrogen oxidation should then be the sum of the current density from the oxidation of each type of adsorbed H, i.e.,

$$j = \sum j_i \quad (10)$$

where i = weak, strong.

When the dissociative adsorption reactions are the rate-determining steps, the corresponding current density can be expressed as,

$$j_i = 2F[k_{m,i} c_{H_2^s} (\theta_i^* - \theta_i)^m - k_{m,i-} (\theta_i)^m (c_{H^+})^{2-m}] \quad (11)$$

where $c_{H_2^s}$ represents the concentration of hydrogen molecules in the vicinity of the electrode surface; c_{H^+} is the concentration of H^+; θ_i and θ_i^* represent the coverage of the ith type of adsorbed H and its saturation value. The forward ($k_{m,i}$) and reverse ($k_{m,i-}$) rate constants are specified for the reaction of the ith species. These rate constants are also characterized by the reaction mechanism under consideration, m = 2 or 1 for

the Tafel−Volmer or the Heyrovsky−Volmer reaction mechanism, respectively. The concentration polarization of H^+ is negligible since its bulk concentration is much higher than that of the hydrogen molecule. At the equilibrium potential, the current densities associated with the forward and backward reactions are both equal to the corresponding exchange current density $j_{0,i}$ (i.e. $j_{0,\mathrm{weak}}$ is the exchange current density of the weakly adsorbed hydrogen and $j_{0,\mathrm{strong}}$ is the exchange current density for the strongly adsorbed hydrogen), i.e.,

$$j_{0,i} = 2Fk_{m,i}^{\mathrm{eq}}\, c_{\mathrm{H}_2^{\mathrm{s}}}(\theta_i^* - \theta_i^{\mathrm{eq}})^m = 2Fk_{m,i-}^{\mathrm{eq}}(\theta_i^{\mathrm{eq}})^m(c_{\mathrm{H}^+})^{2-m} \quad (12)$$

The superscript "eq" represents the values of the corresponding items at the equilibrium potential. Combing eq 10−12 leads to

$$j = \sum\left\{ j_{0,i}\frac{(\theta_i^* - \theta_i)^m}{(\theta_i^* - \theta_i^{\mathrm{eq}})^m}\frac{k_{m,i}}{k_{m,i}^{\mathrm{eq}}}\left[\frac{c_{\mathrm{H}_2^{\mathrm{s}}}}{c_{\mathrm{H}_2^*}} - \frac{(\theta^* - \theta^{\mathrm{eq}})^m(\theta_i)^m}{(\theta^* - \theta)^m(\theta_i^{\mathrm{eq}})^m}\frac{k_{m,i}^{\mathrm{eq}}k_{m,i-}}{k_{m,i}k_{m,i-}^{\mathrm{eq}}}\right]\right\} \quad (13)$$

Assuming that H atoms obey the Frumkin adsorption isotherm on the surface of the Pt electrode, we can express the rate constant of the dissociative reactions in the following general forms,

$$k_{m,i} = k_{m,i}^{\mathrm{eq}}\mathrm{e}^{[(2-m)\beta F/RT]\eta}\mathrm{e}^{\gamma_i f_i(\theta_i - \theta_i^{\mathrm{eq}})} \quad (14)$$

$$k_{m,i-} = k_{m,i}^{\mathrm{eq}}\mathrm{e}^{[-(2-m)(1-\beta)F/RT]\eta}\mathrm{e}^{-(1-\gamma_i)f_i(\theta_i - \theta_i^{\mathrm{eq}})} \quad (15)$$

where η is the overpotential. The first exponential term in the above two rate constant expressions describe how overpotential affects the rate of the electron-transfer process via a Butler−Volmer-type expression. The second exponential term describes the change of the adsorption free energy with the surface coverage of adsorbates, in which f_i is a dimensionless parameter that determines the rate and direction of the change of adsorption free energy with coverage. $f_i > 0$ means a lateral attractive interaction between the neighboring H atoms, $f_i < 0$ means repulsion interaction, and $f_i = 0$ means a Langmuirian adsorption mode. The β and γ_i parameters are the corresponding symmetry factors. Because the Tafel reaction involves no electron-transfer process, the first exponent is ignored in that mechanism. For simplicity, we presume that the two different types of adsorbed hydrogen (strong, weak) do not interact with each other. This assumption is reasonable considering the moderate energetic separation between the two different states (∼150 mV).

The ratio between the concentration of hydrogen in the vicinity of the platinum surface and that in the bulk solution is[2]

$$\frac{c_{\mathrm{H}_2^{\S}}}{c_{\mathrm{H}_2^*}} = 1 - \frac{j}{j_{\mathrm{dL}}} \quad (16)$$

where j_{dL} is the limiting diffusion current density as defined in eq 5. Since both the ionization of the adsorbed H and the discharge of the hydrogen ion on Pt are very fast reactions, the Volmer reaction can be approximately considered being in equilibrium. So, the coverage can be related to the interfacial potential according to the Frumkin isotherm, i.e.,

$$E = E^0 - \frac{RT}{F}f_i(\theta_i^0 - \theta_i) + \frac{RT}{F}\ln\frac{(\theta_i^* - \theta_i)c_{\mathrm{H}^+}}{\theta_i} \quad (17)$$

where E^0 and θ_i^0 are the standard equilibrium potential of the H_2 electrode and the coverage of the ith species at this potential. So,

$$\eta = E - E^{\mathrm{eq}} = \frac{RT}{F}f_i(\theta_i - \theta_i^{\mathrm{eq}}) + \frac{RT}{F}\ln\frac{(\theta_i^{\mathrm{eq}})(\theta_i^* - \theta_i)}{(\theta_i)(\theta_i^* - \theta_i^{\mathrm{eq}})} \quad (18)$$

Substituting eqs 14, 15, 16, and 18 into eq 13 gives a general polarization equation for the *hor*,

$$\frac{j}{j_{\mathrm{dL}}} = \frac{1 - \mathrm{e}^{(-2F/RT)\eta}}{1 + \dfrac{j_{\mathrm{dL}}}{\sum\left[j_{0,i}\dfrac{(\theta_i^* - \theta_i)^m}{(\theta_i^* - \theta_i^{\mathrm{eq}})^m}\mathrm{e}^{\gamma_i f_i(\theta_i - \theta_i^{\mathrm{eq}})}\right]}\mathrm{e}^{[-(2-m)\beta F/RT]\eta}} \quad (19)$$

It can be seen from eq 19 that no Tafel-type relationship between the current and overpotential may be found in the *hor*. The polarization behavior is complicated by the similarity in rate of the forward and backward reactions and also by the different potential dependence of the coverage of each of the reaction intermediates. Thus, one has to be cautious in extracting kinetic and mechanistic information for the *hor* using Tafel plots.[5−7] The Tafel current−potential relationship is actually an approximation of the Butler−Volmer equation that describes how the rate of an electron (or ion) transfer reaction may be modified by the interfacial potential drop.[2,49,50] As the contribution to the current from the reverse process of an electron-transfer reaction is negligible, the Butler−Volmer equation simplifies to the Tafel relationship, the empirically semilogarithm expression between the current and overpotential first drawn by Tafel from the polarization data obtained for the *her*.[51] As can be seen in the reaction sequences shown above in eqs 6−8, the *hor* is a preceding adsorption−electron-transfer coupled reaction. In the case where a reaction involves electron-transfer coupled with preceding chemical transformation steps for which the latter step is the rate-determining step, the steady-state polarization behavior would be very similar to that of a diffusion-controlled reaction, i.e.,

$$\eta = -\frac{RT}{nF}\ln\left(1 - \frac{j}{j_{\mathrm{L}}}\right) \quad (20)$$

but the limiting current density j_{L} in eq 20 is due to the limiting rate of the preceding chemical process rather than the true liming diffusion rate. In this case there would be no reason to expect a Tafel-type relationship between the current and the overpotential.

At this point a question may be asked as to why the Tafel plot can be used in electrokinetic and mechanistic analysis of the *her*. The answer to this is that in the *her* the process is a following desorption step coupled to an electron-transfer reaction, and so is more easily decoupled. The following chemical transformation coupled with an electron-transfer reaction should exhibit a polarization behavior very similar to that of a simple electron-transfer process, and thus can be described by the Tafel relationship if the back reaction can be ignored. A detailed analysis of the polarization behavior of coupled electron-transfer reactions may be found in many textbooks of electrochemistry.[2,49,50]

It is also worthwhile to comment on the commonly used equation

$$\frac{1}{j} = \frac{1}{j_k} + \frac{1}{j_{\mathrm{dL}}} \quad (21)$$

which has been frequently used to extract kinetic parameters in many RDE studies of the *hor* in the literature, where j_k refers to the current density in the absence of any concentration depletion occurring.[5−7,18,42] This equation is only valid when the rate of the back reaction in the rate-determined step is negligible. At least at low overpotentials, the contribution from the back reactions in the adsorption steps (eqs 6 and 7) in the *hor* is significant. In these cases the corresponding equation including the contribution from the back reaction should be,

$$\frac{1}{j} = \frac{1}{j_k} + \frac{1}{j_{dL}} \frac{kc_{H_2^*}}{j_k} \tag{22}$$

where k is the rate constant of the forward reaction of the rate-determining step, which may be both potential and coverage dependent as adsorption processes are involved in the reaction. Equation 22 has been derived by assuming that there is no concentration polarization of hydrogen ion in the solution. Only as

$$j_k \rightarrow kc_{H_2^*} \tag{23}$$

i.e., as the back reaction becomes negligible, can eq 22 be simplified to eq 21. In a recent paper by Wang et al.,[42] the authors realized that the contribution of the back reaction could not be ignored in the *hor* and therefore substituted j_k by the full Butler−Volmer equation in eq 21 to derive a polarization equation for the *hor*. Two mistakes have been made by doing so. First, eq 21 itself is valid only when the back reaction can be ignored. Thus, eq 22 should be used as the starting equation. Second, j_k for the *hor* should not have a Butler−Volmer-type dependence on the overpotential as discussed above.

In contrast eq 19 has been derived with a more realistic set of assumptions: that the rate constants of the forward and backward reactions are similar and that two different forms of adsorbed atomic H need to be considered. This equation should be able to be applied to the steady-state polarization for the *hor* on electrodes of various electrocatalytic materials.

3.3. The Reaction Mechanism of the hor. As shown in Figure 1, the major feature in the kinetics of the *hor* is that of an extra limiting current occurring in the steady-state curves as the electrode size decreases to submicrometer dimensions. The limiting current accompanying an electrochemical process should be caused by the limiting rate of a step preceding the electron-transfer process. The rates of such preceding steps are either potential independent or change little with potential relative to the electron-transfer process. In most cases, the preceding step that is responsible for the limiting current is the diffusion of the electroactive species toward the electrode/electrolyte interface. In addition, a limiting current may also be exhibited in a preceding heterogeneous chemical transformation step coupled to a rapid electron-transfer reaction.[2,49,50] As shown in the above reaction sequences (eqs 6−8), the Tafel−Volmer reaction sequence is an example of a mechanism containing a rapid electron-transfer reaction coupled with a preceding chemical adsorption step. It is our hypothesis that the extra limiting current plateau on the steady-state polarization curves obtained on small particle electrodes is due to the limiting rate of the Tafel step. That is, that the *hor* on Pt electrodes may proceed via the Tafel−Volmer reaction mechanism. Since the Heyrovsky step is a combined chemical−electrochemical process, the reaction rate would vary significantly with increasing overpotential and tend to not show a limiting value. For the Heyrovsky−Volmer mechanism a limiting current may only occur due to diffusion limiting behavior.

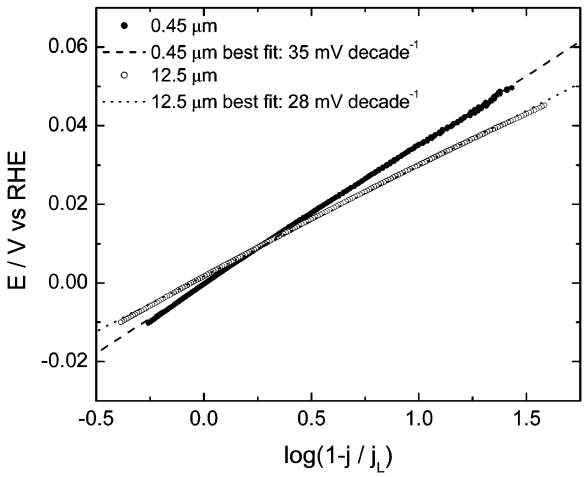

Figure 2. Plots of E vs $\log(1 - j/j_L)$ for the *hor* in 0.1 mol dm^{-3} H_2SO_4 solution saturated with CO free hydrogen gas under steady-state conditions on a Pt microdisk electrode of 12.5 μm radius (○) and a Pt particle electrode of 0.45 μm radius (●). Best fit lines for the data are also provided.

As shown in eq 20, there should be a linear relationship between the overpotential and the value of $\log(1 - j/j_L)$ for a preceding chemical adsorption controlled reaction where j_L is due to the limiting rate of adsorption. In Figure 2, two examples of the η vs $\log(1 - j/j_L)$ lines obtained from the steady-state polarization curves accompanying *hor* on the single Pt particle electrodes are given. The limiting current j_L can be read from the current plateau values at about 0.1 V in Figure 1. It can be seen that good linear relationships between η vs $\log(1 - j/j_L)$ can be found in the potential region between −0.01 and 0.05 V. The slopes are close to 30 mV decade^{-1}, agreeing well with the predictions of eq 20 with $n = 2$ for the oxidation of a hydrogen molecule. This seems also to confirm that the *hor* on polycrystalline Pt electrodes undergoes the Tafel−Volmer reaction sequence. We have also tried to fit the data with the Tafel relationship but no reasonable linear response can be fitted on the plot of η vs $\log[(j^* j_{dL}/(j_{dL} - j)]$ in the potential region below 0.1 V.

If we let

$$j_L = \frac{j_{dL}}{1 + \dfrac{j_{dL}}{\sum\left[j_{0,i} \dfrac{(\theta_i^* - \theta_i)^2}{(\theta_i^* - \theta_i^{eq})^2} e^{\gamma_i f_i (\theta_i - \theta_i^{eq})}\right]}} \tag{24}$$

then eq 19 for the Tafel−Volmer mechanism (i.e., $m = 2$) becomes identical to eq 20. This says that the limiting current plateau at lower potentials can be described by eq 24 under the Tafel−Volmer reaction mechanism. Equation 24 can then be obtained from eq 19 as

$$1 - e^{(-2F/RT)\eta} \approx 1 \tag{25}$$

Equation 25 may be satisfied at $\eta < 50$ mV, exactly at those potentials where the lower potential limiting current plateau is established in the polarization curves for small particle electrodes.

Equation 24 also implies that the limiting current plateau occurring at lower potentials is not solely caused by the adsorption. Instead, it is a result of combined adsorption and

diffusion. Equation 24 can be expressed in the same form as eq 21 by setting

$$j_k = \sum\left[j_{0,i} \frac{(\theta_i^* - \theta_i)^2}{(\theta_i^* - \theta_i^{eq})^2} e^{\gamma_i f_i(\theta_i - \theta_i^{eq})} \right] \qquad (26)$$

Here j_k represents the kinetic current density associated with the dissociative adsorption without concentration polarization. When the value of j_{dL} is very small, e.g., if electrodes of large radii are used, the limiting current will become approximately equal to the limiting diffusion current. This is why the two limiting current plateaus become less separated with increasing electrode size. Furthermore, the limiting current may also merge into the diffusion limiting current if j_k is significantly increased. This may be the reason for the occurrence of the limiting current at higher overpotential.

Since the value of θ_i will vary continuously with potential, j_k would vary continuously according to eq 26. Thus, there would be no true limiting current established before the reaction becomes diffusion limited even for the Tafel−Volmer reaction mechanism. The limiting current plateau at around 0.1 V may be due to the compensatory effects of the $(\theta_i^* - \theta_i)^2$ and $e^{\gamma_i f_i(\theta_i - \theta_i^{eq})}$ terms so that j_k changes relatively slowly with potential. On relatively large particles for which the j_{dL} values are small, the limiting current will be predominantly controlled by j_{dL} so that the overall current changes little with potential. Indeed, this is seen in the polarization curves in Figure 1. It can be seen that the plateau at lower potentials becomes better defined on larger particles. On very small particles, the limiting plateau becomes ill defined since on these electrodes the value of j_{dL} is increased and the relative contribution of j_k to the overall current becomes more pronounced.

To confirm the above mechanistic analysis, we have tried to simulate the experimental polarization data with the full expression of eq 19. In performing these simulations, we assume that there are two types of adsorbed H atoms, the strongly bound H and weakly bound H, serving as the reactive intermediates. To obtain the coverage of each type of the UPD H, cyclic voltammograms in the H UPD region of a large electrode in H_2 free sulfuric acid solution were deconvoluted into two separate peaks by assuming that the current wave associated with the adsorption of each atomic H is symmetric with respect to each of those peaks. The negative going scan was used for this purpose, and the hydrogen evolution wave was subtracted from the adsorption currents. The deconvolution process is seen in Figure 3. The resulting fit to the hydrogen adsorption region is very good, and the resulting total integrated hydrogen adsorption charge is very similar to that reported by others.

We avoided using the cyclic voltammograms obtained on the very small particles because of the low signal/noise ratio of the measured current. For example, the peak current associated with the UPD adsorption/desorption on the smallest particle is only a few picoamperes in magnitude even at a scan rate of 1000 mV s^{-1}, although the two peaks are clearly seen and well defined. We found that the adsorption peaks can be very well fitted by Lorenzian-type peaks. Although it may be possible to provide better fits to the hydrogen adsorption region by using different peak shapes or increasing the number of peaks, we feel that this approach represents the simplest tactic to the deconvolution of the different states of adsorbed hydrogen.

Utilizing eq 19 and the deconvoluted coverages for strongly and weakly adsorbed hydrogen reasonable fits to the data can be achieved by setting $m = 2$ in eq 19, i.e., assuming a Tafel−Volmer reaction mechanism. The fitting results are shown in Figure 4, and the parameters required for the best fits are listed in Table 3.

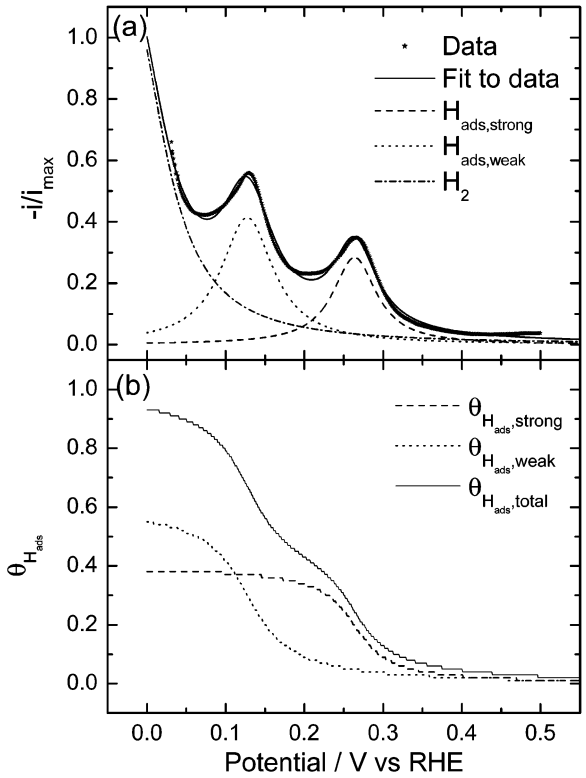

Figure 3. Deconvolution of the hydrogen adsorption region into strongly adsorbed hydrogen (- - -), weakly adsorbed hydrogen (···), and H_2 evolution (· − · −) (a). Original data (•) obtained on a polycrystalline Pt RDE in N_2 saturated 0.1 mol dm^{-3} H_2SO_4, $\omega = 1000$ rpm, 20 mV s^{-1}; total fit to the data (—) are also shown. (b) Corresponding coverages of weakly adsorbed hydrogen (···), strongly adsorbed hydrogen (- - -), and total adsorbed hydrogen coverage (—), obtained by integration of the results in part a.

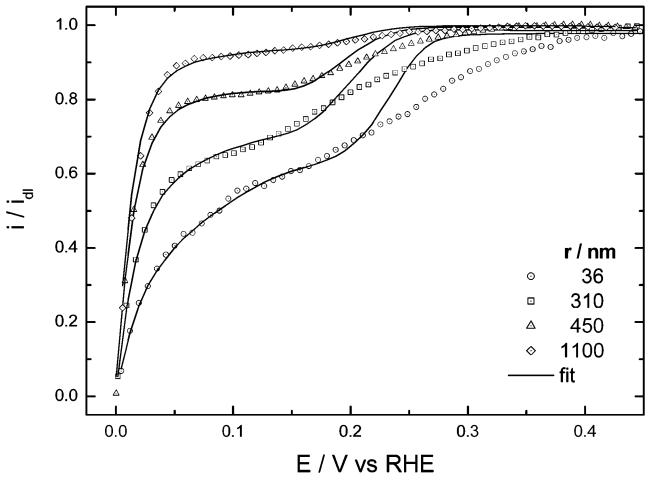

Figure 4. Experimental fits, using eq 19, to the data in Figure 1 assuming a Tafel−Volmer reaction mechanism ($m = 2$). The fitting parameters are listed in Table 3.

It can be seen that in all cases the theoretical curves show an approximate limiting plateau in the lower potential region. The corresponding fitting parameters are reasonably close for particles of different size, with the largest deviations from the mean values seen on the smallest particle. The values of the exchange current density are very close to those determined from the slope of $j \sim \eta$ lines near equilibrium potentials (see the next section). It can be seen that the theoretical curves

TABLE 3: Parameters Used To Fit the Polarization Curves in Figure 4

r/nm	m/cm s^{-1}	$(\theta^* - \theta^{eq})_{weak}$	$(\theta^* - \theta^{eq})_{strong}$	$j_{0,weak}$/mA cm^{-2}	$j_{0,strong}$/mA cm^{-2}	γf_{weak}	γf_{strong}
36	10.3	1.5×10^{-2}	8×10^{-3}	8.8	17	2.9	4
310	1.2	1.5×10^{-2}	8×10^{-3}	3.3	17	4.2	10
450	0.82	1.5×10^{-2}	8×10^{-3}	4.5	17	5.1	10
1100	0.34	1.5×10^{-2}	8×10^{-3}	4.1	17	4	10

generally deviate from the experiment curves as $\eta > 0.25$ V. In the theoretical model, we have supposed that H atoms from the dissociation of a hydrogen molecule occupy the sites of the same state:

$$H_2^s + Pt \underset{k_{1,weak-}}{\overset{k_{1,weak}}{\rightleftharpoons}} 2Pt\text{-}H_{weak} \tag{27}$$

and

$$H_2^s + Pt \underset{k_{1,strong-}}{\overset{k_{1,strong}}{\rightleftharpoons}} 2Pt\text{-}H_{strong} \tag{28}$$

In reality, it may be possible that the two atoms go to different types of surface sites:

$$H_2^s + Pt \underset{k_-}{\overset{k}{\rightleftharpoons}} Pt\text{-}H_{weak} + Pt\text{-}H_{strong} \tag{29}$$

At lower potentials, the sites for strongly bound H are almost fully occupied, and the adsorption will mainly take place on the sites for weakly bound H. The theoretical model thus is more applicable at lower overpotentials, i.e., at $E < 0.2$ V. At more positive potentials, both types of surface sites are available for hydrogen adsorption and the cross adsorption process may become significant. As far as the application to fuel cells is concerned, this is not too serious a limitation, as most fuel cell anodes operate at $E < 0.1$ V.

The theoretical best-fit curves for the Heyrovsky−Volmer mechanism only give relatively poor fits although they do show two approximate plateaus. However, the resultant fitting parameters are rather unrealistic. For example, the fitted values for the exchange current densities are mostly smaller than 10^{-5} A cm^{-2}, and sometimes even negative values are produced. If we constrain the parameters to take on values in a physically reasonable range the fits only produce one limiting current plateau.

3.4. The Exchange Current Density (j_0). Having assigned the reaction mechanism, we are able to extract the exchange current density from the steady-state polarization curves. As discussed in the previous section, the polarization equation for the *hor* cannot be simplified into a linear Tafel equation. An alternative way is to use the linear relationship between the current and the overpotential at very low overpotential region to extract the kinetic parameters. At very low overpotentials, the deviation of the surface coverage of the adsorbed hydrogen species from their equilibrium coverage may be small and negligible, so

$$\theta_i \approx \theta_i^{eq} \tag{30}$$

In addition, a very low value of η (e.g., $\eta < 5$ mV) would render the parameter $(2F/RT)\eta \ll 1$. Under these circumstances eq 19 can be simplified into a linear form,

$$j = \frac{\frac{2F}{RT}\eta}{\frac{1}{j_{dL}} + \frac{1}{j_0}} \tag{31}$$

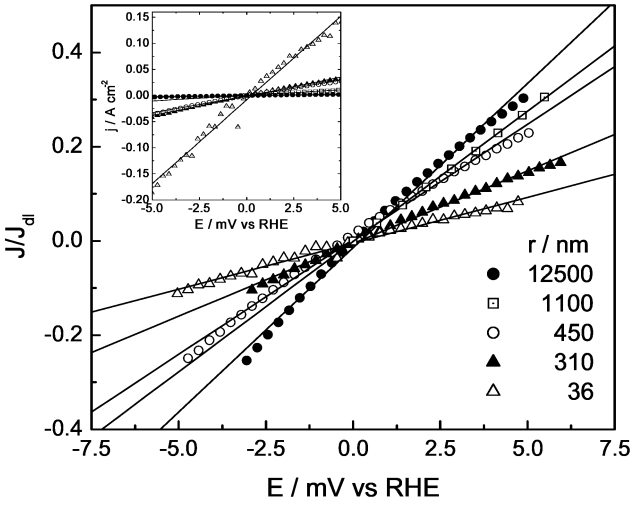

Figure 5. Steady-state polarization curves for the *hor* obtained on Pt particle electrodes of different size in 0.1 mol dm^{-3} H_2SO_4 solution saturated with CO free hydrogen gas. The currents are normalized to the corresponding diffusion-limited current on that electrode. The electrode radii are indicated in the figure. The inset is the corresponding current density data.

where the exchange current density is the sum of the values for the adsorption of each type of adsorbed H:

$$j_0 = \sum j_{0,i} \tag{32}$$

The exchange current density can be determined from the slope of the corresponding $J-\eta$ lines in the region near the equilibrium potential, referred to as the "micropolarization region" by Marković et al.[6] They used the analysis of the current variation in the micropolarization region to determine the exchange current density for the *hor* on Pt single-crystal electrodes in acid solution. The equation used by Marković et al. is obtained directly from the linearization of the Butler−Volmer equation and thus they neglected any possible concentration polarization:

$$j = \frac{j_0 F}{RT}\eta \tag{33}$$

It can be seen from eq 31 that the slope of $J-\eta$ curves near equilibrium potentials for *hor* should be $j_0 j_{dL}/(j_0 + j_{dL})(2F/RT)$ rather than j_0F/RT as determined from eq 33 in the absence of any concentration polarization. Only when the mass transport rate of the system is very high such that $j_0 \ll j_{dL}$ may the concentration polarization be ignored. As shown by eq 19, no linear relation between current and overpotential can be obtained for the Heyrovsky −Volmer mechanism unless the overpotential is extremely small or the mass transport rate of the system is very high so that no concentration polarization occurs.

Figure 5 shows the normalized polarization curves near the equilibrium potential obtained on our Pt particle electrodes. It can be seen that the polarization data are well described by eq 31. Because the current density is normalized by the corresponding limiting diffusion current density, the slope becomes smaller on smaller particles due to the increased value of j_{dL}. It

TABLE 4: Exchange Current Density j_0 Determined from the Steady-State Polarization Curves in the Micropolarization Region According to Eqs 33 and 31, and the Exchange Current Density Determined from the Sum of the Individual Exchange Current Densities Obtained from the Full Fit of the Data by Using Eq 19 (data from Table 3)

	j_0/mA cm^{-2}		
electrode adius/μm	from j_0F/RT [a]	from $[j_0 j_{dL}/(j_0 + j_{dL})][2F/RT]$ [b]	from $j_{0,weak} + j_{0,strong}$ [c]
12.5[d]	12	19	22
1.1	54	40	21
0.45	160	29	23
0.31	188	22	21
0.036	840	23	20

[a] Micropolarization region assuming Butler−Volmer kinetics. [b] Micropolarization region assuming eq 31 (from eq 19). [c] Full fit of the entire steady-state polarization plot to eq 19. [d] Disk electrode.

can be seen that the current reaches a value of about 20% of the limiting diffusion current at an overpotential of 5 mV on the particle of about 0.45 μm in radius, and about 30% on the electrode of 12.5 μm. One has to consider the contribution of concentration depletion to the polarization curve in such cases. On a particle of about 36 nm, the current density at $\eta = 5$ mV is less than 10% of the limiting diffusion current. Only in this case may one ignore the mass transport effect, and the calculated j_0 value changes little when ignoring the diffusion contribution in eq 31.

Table 4 gives the values of exchange current densities determined from the polarization curves obtained on Pt particle electrodes of different size using eqs 31 and 33 and the slopes in Figure 5. The values of j_0 determined by using eq 33 vary by over 1 order of magnitude on the particles studied. In comparison, the value of j_0 determined by using eq 31 varies little with particle size and shows an average value of j_0 of about 27 mA cm^{-2}. For comparison, the value of j_0 determined from the sum of the individual $j_{0,i}$ values according to eq 32 and utilizing the total fits of the experimental data to eq 19 (Figure 4) are also displayed (i.e., the sum of the j_0 values in Table 3). There is very good agreement between the j_0 values determined by using eq 19 and the micropolarization linear region according to eq 31, with the combined j_0 value being 24 mA cm^{-2}.

This value is in good agreement with the values measured with use of rapid potentiodynamic scanning, thin liquid layer microelectrode, and SECM methods, but much higher than that measured with use of the RDE method (see Table 1). As shown in the Introduction, measurements made by using the RDE method at room temperature may be severely affected by the low mass transport rate achievable by this technique. The value of the sum of the exchange current density values thus determined is also close to those fitting parameters in the previous section as the Tafel−Volmer reaction mechanism is assumed.

4. Conclusion

The electrochemical oxidation of hydrogen on polycrystalline Pt in a sulfuric acid solution has been studied by using electrodes made of single Pt particles supported on carbon. The single particle electrodes with submicrometer size provide very high mass transport rate allowing the mechanism and kinetics of the *hor* to be clearly revealed, especially in the H UPD region.

We consider that H produced from the adsorption of H_2 is indistinguishable from H produced from the UPD process. The presence of H_2 in solution adjacent to the Pt surface perturbs the coverage of H above its equilibrium value at that potential, and this accelerates the Volmer process which tries to reestablish the H coverage to its equilibrium value. Steady-state polarization curves with two limiting current plateaus were obtained when using single particle electrodes of submicrometer dimensions. Such polarization behavior of the *hor* can be explained with the Tafel−Volmer reaction mechanism, but not the Heyrovsky−Volmer mechanism. Hence it is the H_2 adsorption process that is the slow step during hydrogen oxidation, and variations in the rate of the hydrogen oxidation rate with potential are due to the change in the number of free adsorption sites with potential. It is necessary to consider both weakly and strongly adsorbed H as distinct species with independent exchange current densities and interaction parameters.

We have modeled the steady-state hydrogen oxidation process and shown that the first current plateau in the steady-state polarization curves on small particle electrodes is due to the limiting rate of the Tafel reaction. We have also shown that it is unwise to use Tafel plots in performing the kinetic and mechanistic analysis of the *hor* since it is a preceding chemical adsorption coupled electron-transfer reaction. In contrast to a recent model for the *hor* by Marković et al.,[5−7] we conclude that the UPD H could be the reaction intermediate rather than an inhibitor of the *hor*.

Most previous work on the *hor* has assumed that the reaction is governed by relatively simple kinetics. In contrast, we have shown that to fully understand this reaction, it is necessary to have some knowledge about the mass transport process at the platinum electrode. This has implications for both understanding and modeling and the *hor* in solid polymer electrolyte fuel cells (SPFC): in an SPFC the *hor* will be controlled by the local mass transport coefficient of hydrogen, and any realistic model (or calculation of, for instance j_0) needs to include some measure of that parameter.

Acknowledgment. Financial support for this research is from the Leverhulme trust. We thank Mr. Peter Hope from LVH for kindly providing the electrophoretic paint solution. Mr. Simon Turner and Mr. Steve Atkins in the Chemistry Department of this college are thanked for their technical support.

References and Notes

(1) Gottesfeld, S.; Zawodzinski, T. A. Polymer Electrolyte Fuel Cells. In *Advance in Electrochemical Science and Engineering*, 1st ed.; Alkire, R. C., Gerischer, H., Kolb, D. M., Tobias, C. W., Eds.; Wiley-VCH: Weinheim, Germany, 1997; Vol. 5, p 195.

(2) Bard, A. J.; Faulker, L. R. *Electrochemical Methods*, 1st ed.; John Wiley: New York, 1980.

(3) Harrison, J. A.; Khan, Z. A. *J. Electroanal. Chem.* **1971**, *30*, 327.

(4) Makowski, M. P.; Heitz, E.; Yeager, E. *J. Electrochem. Soc.* **1966**, *113*, 204.

(5) Marković, N. M.; Sarraf, S. T.; Gasteiger, H. A.; Ross, P. N. *J. Chem. Soc., Faraday Trans.* **1996**, *92*, 3719.

(6) Marković, N. M.; Grgur, B. N.; Ross, P. N. *J. Phys. Chem. B* **1997**, *101*, 5405.

(7) Schmidt, T. J.; Ross, P. N.; Marković, N. M. *J. Electroanal. Chem.* **2002**, *524−525*, 252.

(8) Maruyama, J.; Inaba, M.; Katakura, K.; Ogumi, Z.; Takehara, Z. *J. Electroanal. Chem.* **1998**, *447*, 201.

(9) Mello, R. M. Q.; Ticianelli, E. *Electrochim. Acta* **1997**, *42*, 1031.

(10) Bagotzky, V. S.; Osetrova, N. V. *J. Electroanal. Chem.* **1973**, *43*, 233.

(11) Kita, H.; Ye, S.; Gao, Y. *J. Electroanal. Chem.* **1992**, *334*, 352.

(12) Gomez, R.; Fernandez-Vega, A.; Felui, J. M.; Aldaz, A. *J. Phys. Chem. B* **1993**, *97*, 4769.

(13) Vogel, W.; Lundquist, J.; Ross, P.; Stonehart, P. *Electrochim. Acta* **1975**, *20*.

(14) Zoski, C. G. *J. Phys. Chem. B* **2003**, *107*, 6401.

(15) Zhou, J. F.; Zu, Y. B.; Bard, A. J. *J. Electroanal. Chem.* **2000**, *491*, 22.

(16) Mirkin, M. V.; Bard, A. J. *Anal. Chem.* **1992**, *64*, 2293.

(17) Oldham, K. B. Steady-State Voltammetry. In *Microelectrode*: *Theory and Application*; Montenegro, M. I., Queiros, M. A., Daschbach, J. L., Eds.; Kluwer: The Netherlands, 1991; p 35.
(18) Gasteiger, H. A.; Marković, N. M.; Ross, P. N. *J. Phys. Chem.* **1995**, *99*, 8290.
(19) Jambunathan, K.; Shah, B. C.; Hudson, J. L.; Hillier, A. C. *J. Electroanal. Chem.* **2001**, *500*, 279.
(20) Mirkin, M. V.; Richards, T. C.; Bard, A. J. *J. Phys. Chem.* **1993**, *97*, 7672.
(21) Shuldiner, S. *J. Electrochem. Soc.* **1960**, *107*, 452.
(22) Conway, B. E.; Tilak, B. V. *Electrochim. Acta* **2002**, *47*, 3571.
(23) Conway, B. E.; Barber, J.; Morin, S. *Electrochim. Acta* **1998**, *44*, 1109.
(24) Conway, B. E.; Jerkiewicz, G. *Electrochim. Acta* **2000**, *45*, 4075.
(25) Conway, B. E.; Bai, L. *J. Electroanal. Chem.* **1986**, *198*, 149.
(26) Conway, B. E.; Bai, L. *J. Chem. Soc., Faraday Trans.* **1985**, *81*, 1841.
(27) Conway, B. E.; Jerkiewicz, G. *Solid State Ionics* **2002**, *150*, 93.
(28) Bewick, A.; Taxford, A. M. *J. Electroanal. Chem.* **1973**, *47*, 255.
(29) Bewick, A.; Russell, J. W. *J. Electroanal. Chem.* **1982**, *132*, 329.
(30) Nichols, R. J.; Bewick, A. *J. Electroanal. Chem.* **1988**, *243*, 445.
(31) Bewick, A.; Russell, J. W. *J. Electroanal. Chem.* **1982**, *142*, 337.
(32) Protopopoff, E.; Marcus, P. *J. Vac. Sci. Technol.* **1987**, *A5*, 944.
(33) Protopopoff, E.; Marcus, P. *J. Chim. Phys. Phys. Chim. Biol.* **1991**, *88*, 1423.
(34) Penner, R. M.; Heben, M. J.; Longin, T. L.; Lewis, N. S. *Science* **1990**, *250*, 1118.
(35) Slevin, C. J.; Gray, N. J.; Macpherson, J. V.; Webb, M. A.; Unwin, P. R. *Electrochem. Commun.* **1999**, *1*, 282.
(36) Conyers, J. L.; White, H. S. *Anal. Chem.* **2000**, *72*, 4441.
(37) Chen, S. L.; Kucernak, A. *Electrochem. Commun.* **2002**, *4*, 80.
(38) Chen, S. L.; Kucernak, A. *J. Phys. Chem. B* **2002**, *106*, 9396.
(39) Chen, S. L.; Kucernak, A. *J. Phys. Chem. B* **2003**, *107*, 8392.
(40) Chen, S. L.; Kucernak, A. *J. Phys. Chem. B* **2004**, accepted for publication.
(41) Pozio, A.; Giorgi, L.; Antolini, E.; Passalacqua, E. *Electrochim. Acta* **2000**, *46*, 555.
(42) Wang, J. X.; Brankovic, S. R.; Zhu, Y.; Hanson, J. C.; Adzic, R. R. *J. Electrochem. Soc.* **2003**, *150*, A1108.
(43) Notoya, R.; Matsuda, A. *J. Phys. Chem.* **1989**, *93*, 5521.
(44) Woods, R. Chemisorption at Electrodes: Hydrogen and Oxygen on Noble Metals and Their Alloys. In *Electroanalytical Chemistry*; Bard, A. J., Ed.; Marcel Dekker: Inc.: New York, 1976; Vol. 9, p 27.
(45) Breiter, M. W. *J. Electroanal. Chem.* **1964**, *8*, 449.
(46) Mignolet, J. C. P. *J. Chem. Phys.* **1951**, *54*, 19.
(47) Aston, J. G. *J. Phys. Chem.* **1963**, *67*, 2042.
(48) Zolfaghari, A.; Chayer, M.; Jerkiewicz, G. *J. Electrochem. Soc.* **1997**, *144*, 3034.
(49) Thirsk, H. R.; Harrison, J. A. *A Guide to the Study of Electrode Kinetics*; Academic Press: New York, 1972.
(50) *Instrumental Methods in Electrochemistry/Southampton Electrochemistry Group*; Horwood Publishing: Chichester, UK, 1985.
(51) Tafel, J. *Z. Phys. Chem.* **1905**, *50A*, 641.